Processing and Application of Ceramics 12 [3] (2018) 268–276
https://doi.org/10.2298/PAC1803268R

Ag^+, Cu^{2+} and Zn^{2+} doped hydroxyapatite/tricalcium phosphate bioceramics: Influence of doping and sintering technique on mechanical properties

Željko Radovanović[1,*], Đorđe Veljović[2], Lidija Radovanović[1], Ilmars Zalite[3], Eriks Palcevskis[3], Rada Petrović[2], Đorđe Janaćković[2]

[1]*University of Belgrade, Innovation Center of Faculty of Technology and Metallurgy, Karnegijeva 4, 11120 Belgrade, Serbia*
[2]*University of Belgrade, Faculty of Technology and Metallurgy, Karnegijeva 4, 11120 Belgrade, Serbia*
[3]*Institute of Inorganic Chemistry, Riga Technical University, Miera 34, Salaspils, LV-2169, Riga, Latvia*

Received 25 May 2018; Received in revised form 18 July 2018; Accepted 20 August 2018

Abstract

Green hydroxyapatite ceramics were obtained by cold uniaxial and isostatic pressing of hydrothermally synthesized powders, pure hydroxyapatite and hydroxyapatite doped with Ag^+, Cu^{2+} and Zn^{2+} ions. The ceramics were conventionally and microwave sintered and analyzed by Fourier transform infrared spectroscopy, field emission scanning electron microscopy, X-ray diffraction analysis, and energy-dispersive X-ray spectroscopy. The effect of doping on the mechanical properties of the obtained hydroxyapatite/tricalcium phosphate ceramics was examined by comparing their average grain size, porosity and values of the hardness and fracture toughness. The results showed that doping with Cu^{2+} ions caused the lowest porosity of the ceramics and the highest values of hardness and fracture toughness. The ceramics obtained from hydroxyapatite doped with Ag^+ and Zn^{2+} ions exhibited worse mechanical properties due to the higher porosity even in the case of microwave sintering, which provide denser ceramics than conventional sintering.

Keywords: *doped apatite, conventional and microwave sintering, microstructure, mechanical properties*

I. Introduction

Calcium phosphates constitute the inorganic part of bones and teeth of mammals. This fact is well known and has encouraged researchers to apply hydroxyapatite (HAp, $Ca_{10}(PO_4)_6(OH)_2$) and α- and β-TCP tricalcium phosphate (TCP, $Ca_3(PO_4)_2$) as implant materials [1,2]. Their similarity to the inorganic part of hard tissues was confirmed [3], highlighting their biocompatibility and osteoconductivity and in addition bioactivity of HAp and bioresorbability of TCP [1,4]. The biphasic forms (BCP): HAp/β-TCP and HAp/α-TCP and triphasic form HAp/β-TCP/α-TCP are of particular interest because they have proved to be even better biomaterials (better bioactivity, bioresorbability, osteoconductivity and osteoinductivity) than the pure, single phase material [4,5]. With careful processing (initial Ca/P ratio, conditions of thermal treatment, etc.), it is possible to obtain the product with required HAp/TCP ratio, regardless of whether it is a powder, compact or scaffold [4,6–8].

Recently, HAp or BCP ceramics were prepared by different sintering methods: microwave sintering (MW) [9–16], conventional sintering (CS) [7,11,16–28], hot pressing (HP) [19,29], hot isostatic pressing (HIP) [7,30] and spark plasma sintering (SPS) [31,32]. Dense sintered forms have suitable values of hardness (H) and fracture toughness (K_{IC}) which makes them appropriate for applications in medicine and stomatology [2,8]. According to the literature [7,10–18,22–32], the maximum values obtained for H and K_{IC} for HAp or BCP ceramics sintered at temperatures of 1000–1400 °C ranged from 2.7 to 6.1 GPa and from 0.9 to 1.58 MPa·m$^{1/2}$, respectively. Previous investigations [14,16,17,25,33] confirmed that the best mechanical properties of HAp/TCP ceramics have been obtained by CS or MW sintering up

*Corresponding authors: tel: +381 11 3303740,
e-mail: *zradovanovic@tmf.bg.ac.rs*

to 1200 °C.

Several authors reported mechanical properties of ceramics obtained using HAp doped with metal ions. Generally, doping of HAp is performed in order to improve its biocompatibility and/or antimicrobial activity [14,16,21,25,32,34–36]. Also, doped HAp ceramics showed better sinterability and mechanical properties than the ceramics made from undoped HAp. The highest values of H for Mn-HAp [14], Zn-BCP [25] and Mg-HAp [32] were 4.80, 3.44 and 5.10 GPa, respectively, while the highest values for K_{IC} were 1.54 [14], 1.43 [25] and 1.00 MPa·m$^{1/2}$ [32].

The aim of this study was to investigate the influence of doping and type of sintering on the microstructure and mechanical properties of HAp/TCP ceramics. The ceramics were prepared from HAp powders doped with Ag^+, Cu^{2+} and Zn^{2+} ions whose antimicrobial activity and biocompatibility were presented earlier [34,35]. The ceramics were sintered by CS at 1200 °C and by MW at 900 and 1200 °C. The temperature of 1200 °C was chosen to compare CS and MW sintering, while MW sintering at 900 °C was applied in order to determine the structure of ceramics at the beginning of sintering. The values of H and K_{IC} for the ceramics were determined.

II. Experimental

2.1. Materials and methods

The ceramics were prepared from the following hydrothermally synthesized powders: HAp, Ag(0.4)HAp, Cu(0.4)HAp and Zn(0.4)HAp [34,35], where 0.4 refers to 0.4 at.% of M (Ag, Cu, Zn) in relation to Ca. The amount of 0.4 at.% of dopant has been chosen because the probability of releasing these ions from ceramics is higher than when a smaller amount of dopant is taken. Hereinafter, the powders are labelled as HAp, AgHAp, CuHAp and ZnHAp, respectively.

The sample preparation was described in detail in our previous papers [34,35]. The pure HAp was synthesized from appropriate quantities of the chemicals: $Ca(NO_3)_2 \cdot 2\,H_2O$, $Na_2H_2EDTA \cdot 2\,H_2O$, $NaH_2PO_4 \cdot 2\,H_2O$ and urea. For the synthesis of the doped HAp, in addition to the aforementioned chemicals, $AgNO_3$ for AgHAp, $Cu(NO_3)_2 \cdot 4\,H_2O$ for CuHAp and $Zn(NO_3)_2 \cdot 6\,H_2O$ for ZnHAp, have been used. The hydrothermal syntheses were performed at 160 °C for 3 h. These powders consisted of rod-like particles agglomerated into a spherical shape. The dimensions of the particles (diameter and/or length) were in the range of a few tens of nanometres to about 1.5 micrometers, depending on whether they were filled or hollow spheres [34,35]. The powders were pressed uniaxially at 100 MPa using a stainless steel die into green disc compacts with the diameter of 8 mm. In addition, the green compacts were isostatically pressed at 400 MPa for 1 min. The first group of obtained ceramics was heated at 10 °C/min and conventionally sintered at 1200 °C for 2 h (ceramics are labelled as follows: H-CS, Ag-CS, Cu-CS and Zn-CS). The second group of ceramics was heated at 20 °C/min and sintered in an automated microwave laboratory furnace (Linn High Therm MHTD 1800-4,8/2,45-135) at 900 and 1200 °C for 15 min (the ceramics of those series were labelled with MW09 or MW instead of CS, respectively).

2.2. Characterizations

Thermal properties of the powders were examined from room temperature up to 1200 °C using an SDT Q600 TGA/DSC instrument (TA Instruments). The heating rate was 20 °C/min and the furnace atmosphere consisted of air at a flow rate of 100 cm^3/min.

Fourier transform infrared spectroscopy (FTIR) was performed using a MB Bomem 100 Hartmann and Braun spectrometer in the wave number range from 4000 to 400 cm^{-1}, using the KBr pellet method.

The morphologies of the ceramics were observed by Tescan Mira 3 FEG field emission scanning electron microscopy (FESEM). Two different surfaces of ceramics were analysed: fracture surface and polished, thermally etched surface (thermally etched for 15 min at temperatures 50 °C lower than the temperatures of sintering). Before analysis, the ceramics were coated with Au-Pd using a Polaron SC502 sputter coater. Average grain sizes (AGS) of the ceramics were determined from the micrographs of the polished and thermally etched surface by a linear intercept method.

Energy-dispersive X-ray spectroscopy (EDS) of the ceramics was performed on a Jeol JSM 5800 SEM with a SiLi X-Ray detector (Oxford Link Isis series 300, UK).

X-ray diffraction patterns of CS ceramics were recorded using a Bruker D8 Advance diffractometer using monochromatized CuKα radiation in the 2θ angle range from 20 to 65° with a step scan of 0.02°. X-ray diffraction patterns of MW09 and MW ceramics were recorded using a Rigaku Ultima IV diffractometer (without monochromator) using CuKα radiation in the 2θ angle range from 20 to 65° with a step scan of 0.02°. Rietveld like analysis of the phases composition in the ceramics were performed by Jade 6 software starting from the X-ray diffraction data and by using standard reference JCPDS cards No: 74-0566, 70-2065 and 29-0359 for HAp, β-TCP and α-TCP, respectively.

The densities of the green compacts (ρ_0) and ceramics (ρ) were determined by measuring the dimensions and weight.

The total porosity (in vol.%) was calculated according to $P = [(V - V_m)/V] \cdot 100$, where V is the volume of the compact and V_m is the volume of the solid phases in the ceramics, which was calculated according to Eq. (1):

$$V_m = \frac{m \cdot H}{TD_{HAp}} + \frac{m \cdot B}{TD_{\beta-TCP}} + \frac{m \cdot A}{TD_{\alpha-TCP}} \qquad (1)$$

where m is the mass of the ceramics; H, B and A are amounts of HAp, β-TCP and α-TCP phases (in wt.%)

respectively, and TD_{HAp}, $TD_{\beta-TCP}$ and $TD_{\alpha-TCP}$ with values of 3.156, 3.067 and 2.863 g cm^{-3} are the theoretical densities of HAp, β-TCP and α-TCP, respectively [16].

The H and K_{IC} values of the ceramics, previously polished, were measured with a Buehler Indentament 1100 series, Vickers Indentation Hardness Tester. The values of K_{IC} were calculated using Eq. (2) [37]:

$$K_{IC} = 0.0824 \cdot M \cdot c^{-3/2} \quad (2)$$

where M is the indentation load and c the length of the induced radial crack. The applied indentation load in the tests was set at 1.0 kg, with a dwell time of 5 s. At least five indentations were made on each sample to obtain an average value of H and K_{IC}.

III. Results and discussion

FTIR analysis (Fig. 1) showed that all characteristic peaks for HAp are identified in spectra of the powders and ceramics [38]. The presence of H_2O is confirmed by the presence of stretching and bending vibrations at 3400 and 1630 cm^{-1}. Symmetric and asymmetric stretching vibrations of PO (ν_1(PO) and ν_3(PO), respectively) were observed at 1090, 1045 and 962 cm^{-1}, whereas the bending vibrations of OPO groups (ν_4 and ν_2) were found at 602, 569 and 472 cm^{-1}. The stretching (ν_S) and liberation (ν_L) vibrations of the OH groups were detected at 3570 and 632 cm^{-1}, respectively. However, some of these vibrations in the spectra of ceramics sintered at 1200 °C were broader or less visible (vibrations of the OH groups), due to the transformation of HAp into TCP during sintering [38–40].

In the spectra of the powders, as well as MW09 ceramics (Fig. 1), the peak at around 880 cm^{-1} representing the $\nu_2(CO_3^{2-})$ bending mode and peaks at 1411, 1457 and 1548 cm^{-1} representing the $\nu_3(CO_3^{2-})$ asymmetric stretching mode, are clearly visible. The presence of CO_3^{2-} ions should be associated with a decomposition of urea, used for the powder synthesis, and these ions were in situ incorporated in the HAp structure [41]. Most of the peaks corresponding to CO_3^{2-} ions are not visible in the spectra of ceramics, because, according to the literature, sintering of HAp powders over 1100 °C leads to the removal of carbonate from the samples [42]. Only a weak peak at about 880 cm^{-1} (CO_3^{2-}) could be observed in the spectra of MW samples but not in the spectra of CS. This is probably due to the faster MW sintering, which does not result in the loss of all CO_3^{2-} ions from the structure of the ceramics.

The FESEM micrographs of fractured and polished surfaces of the ceramics are shown in Fig. 2. Both types of ceramics contain pores that could be described as spherical and shapeless. By comparing the micrographs of the CS and MW ceramics, it is obvious that porosity is lower, i.e. densification is better in the case of MW sintering. Owing to characteristic volumetric heating [17], MW sintering produced denser ceramics for much shorter time (15 min) than conventional sintering for 2 h. As it can be observed from Fig. 2, doping with Ag and Zn caused higher porosity of both types of ceramics (CS and MW), while Cu-doping provided better densification, i.e. lower porosity in comparison to undoped samples. The values of AGS of CS ceramics range from 0.56 to 1.16 μm and increase in order H-CS < Ag-CS < Cu-CS < Zn-CS (Table 1). AGS values of

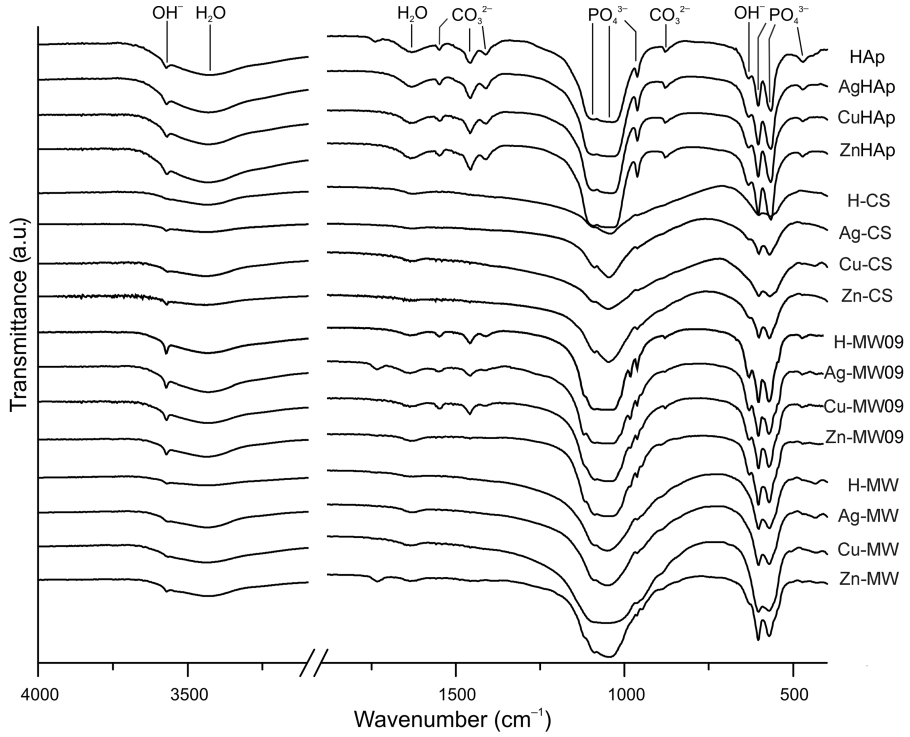

Figure 1. FTIR spectra of powders and ceramics sintered at 1200 °C by CS and at 900 and 1200 °C by MW

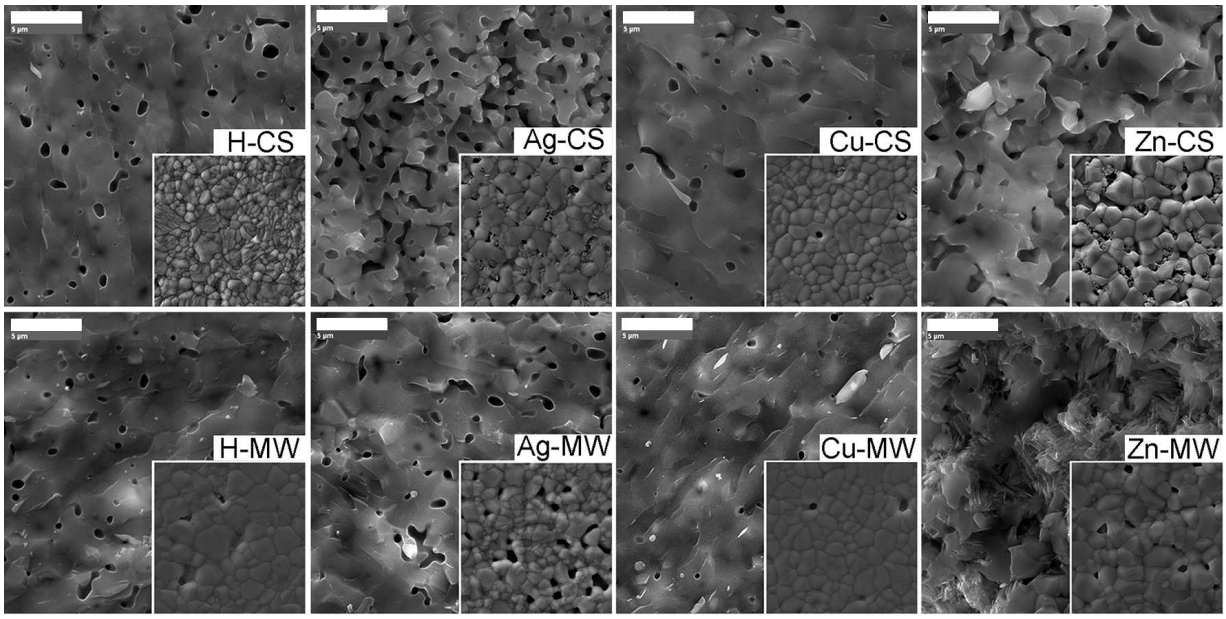

Figure 2. Fracture and polished (small square) surfaces of the ceramics (all figures were recorded at 10000× magnification and the marker bars represent 5 μm)

MW ceramics, with the exception of Ag-MW, were similar and they were about 1 μm (Table 1). The influence of doping on the AGS values was more pronounced for CS series than for MW series, probably due to the longer sintering time. The fracture surfaces indicated predominantly transgranular fracture, which is in accordance with the micrometre size of the grains [19,23,43].

The EDS analyses (Table 1) of the ceramics showed that the Ca/P ratio in all samples was less than the stoichiometric ratio in the pure HAp (1.67), proving the formation of TCP phases. The doped cations were also detected. The atomic proportion of Ag^+ ions was smaller than the atomic proportions of Cu^{2+} and Zn^{2+} ions, indicating that the latter two ions were embedded better into the structure of apatite. According to Nightingale [44], the crystal radii of Ca^{2+}, Cu^{2+}, Zn^{2+} and Ag^+ are 0.099 nm, 0.072 nm, 0.074 nm and 0.126 nm, respectively, and hence, Ag^+ is more difficult to retain in the HAp and TCP structure than Cu^{2+} and Zn^{2+} [35].

XRD patterns of the ceramics (Fig. 3) revealed transformation of HAp into the TCP phases. It is well known that HAp is transformed to β-TCP at temperatures around 800 °C and from β-TCP to α-TCP at about 1100 °C [1,4], which is confirmed by DSC analysis of the HAp powders (Fig. 4). Although the ceramics were sintered at 1200 °C, the transformations HAp → β-TCP and β-TCP → α-TCP are not completed and the ceramics contain all three phases (Fig. 3). The analysis of the XRD data (Table 1) shows that the composition of the ceramics depends on both doping and type of sintering. By comparing H-CS and H-MW, it is obvious that microwave sintering promotes the transformation and stabilization of α-TCP, as it is a case for Ag and Zn samples. Doping with Ag and Zn does not influence significantly the composition of the ceramics, although the content of α-TCP is slightly lower than in undoped samples. On the other hand, the Cu doping stabilize β-TCP phase and the stabilization is more pronounced in the Cu-MW sample than in Cu-CS. Due to the small radius, it is possible that Cu^{2+} interacts more easily with the tetrahedron PO_4^{3-} in the β-TCP, thereby stabilizing it and suppressing the transformation in α-TCP during the shorter MW sintering.

According to the TGA curves (Fig. 4a), the mass loss of all powders was small during heating up to 1200 °C and amounted to about 7%. The DSC results showed

Table 1. Average grain size (AGS), Ca/P ratio including dopant (M) content calculated from EDS results and amount of HAp, β-TCP and α-TCP phases determined from XRD data

Sample	AGS [μm]	(Ca + M)/P [at. ratio]	M [at.%]	HAp [wt.%]	β-TCP [wt.%]	α-TCP [wt.%]
H-CS	0.56 ± 0.05	1.55 ± 0.01	-	29.9(6)	32.2(7)	37.9(8)
Ag-CS	0.86 ± 0.07	1.53 ± 0.02	0.09 ± 0.03	27.3(6)	35.6(7)	37.1(8)
Cu-CS	0.93 ± 0.10	1.59 ± 0.01	0.14 ± 0.04	26.9(4)	44.1(6)	29.0(5)
Zn-CS	1.16 ± 0.18	1.60 ± 0.01	0.14 ± 0.03	37.3(4)	27.2(3)	35.5(4)
H-MW	1.06 ± 0.22	1.60 ± 0.01	-	24.6(4)	26.2(5)	49.2(8)
Ag-MW	0.72 ± 0.10	1.59 ± 0.03	0.07 ± 0.02	30.2(7)	23.8(6)	46.0(9)
Cu-MW	1.03 ± 0.13	1.60 ± 0.01	0.14 ± 0.06	28.5(6)	55.6(9)	15.9(4)
Zn-MW	1.03 ± 0.10	1.57 ± 0.01	0.10 ± 0.04	20.6(5)	36.7(8)	42.7(5)

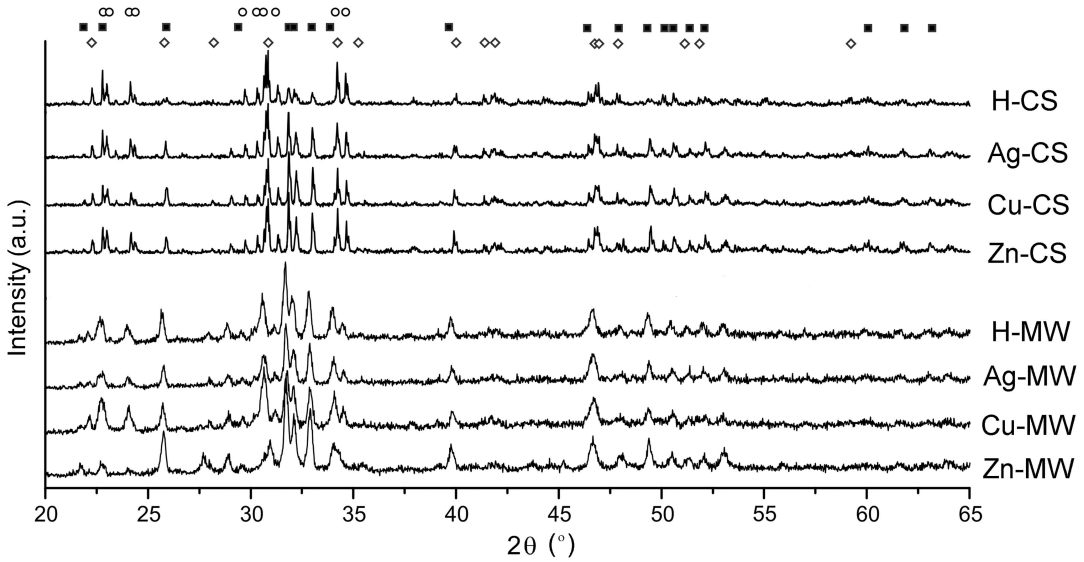

Figure 3. XRD patterns of conventionally and microwave sintered ceramics (the phases HAp, β-TCP and α-TCP are indicated with the symbols ■, ◊ and ○, respectively)

endothermic peaks in the region from 774 to 800 °C, which could be assigned to the transformation of HAp powders into β-TCP (Fig. 4b). On further heating of powders up to 1200 °C, the β-TCP was transformed to α-TCP at about 1100 °C. DSC curves do not show clearly the influence of doping on the temperature of phase transformations.

Mechanical properties, H and K_{IC}, density and porosity of the ceramics are given in Table 2. The highest values of H and K_{IC} for sintered HAp or BCP ceramics obtained previously [7,10–18,22–32] ranged from 2.7 to 6.1 GPa and from 0.9 to 1.58 MPa·m$^{1/2}$, respectively. However, the results have been obtained at different applied loads, and cannot be simply compared. For example, some authors used loads ≤ 500 g [16,17,23–25] to avoid destruction of the samples [23,31], but higher values of H were obtained when lower loads were applied and *vice versa*. In the present research, a load of 1 kg was applied and the values of H and K_{IC} for the undoped samples are relatively high.

The results presented in Table 2 show a clear effect of doping and type of sintering on the mechanical properties of the ceramics. The values of H for Ag-CS and Zn-CS samples are much lower than of H-CS, which is consistent with much higher porosity of doped samples in comparison to undoped one. On the other hand, the doping with Cu had a positive effect on hardness, for both types of sintering. Although the porosity of Zn-MW sample is significantly lower than of Zn-CS, the hardness is not improved, as it is the case of Ag-doped sample. Obviously, some other factors, for example size and shape of pores, influenced the hardness values. It

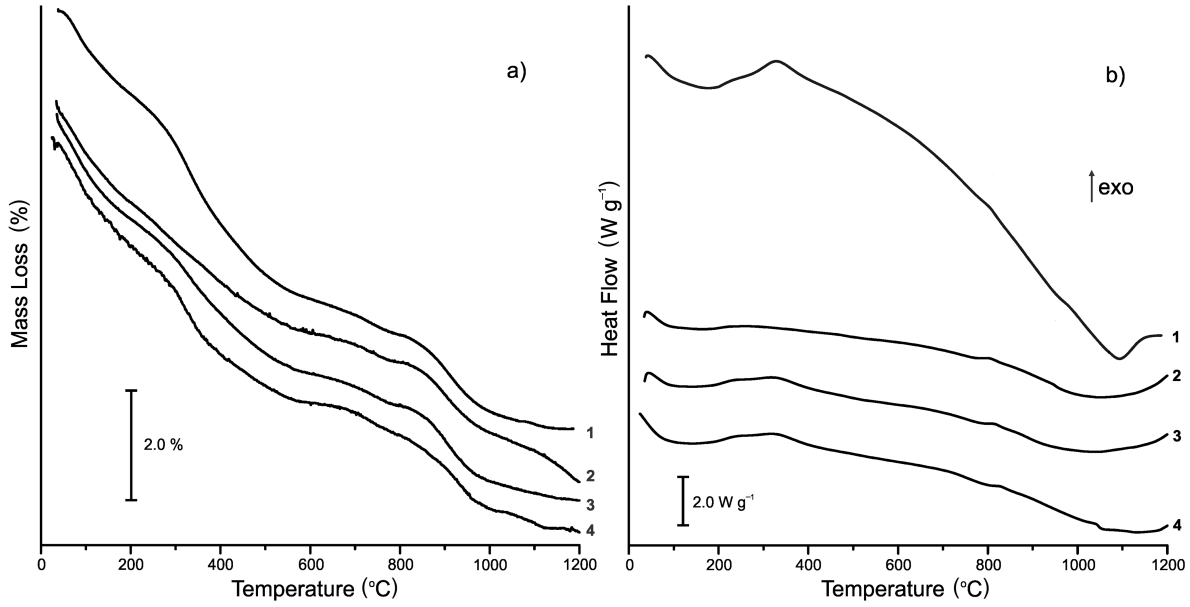

Figure 4. TG (a) and DSC (b) curves for powders: 1-HAp, 2-AgHAp, 3-CuHAp and 4-ZnHAp

Table 2. Hardness (H) and fracture toughness (K_{IC}), initial density (ρ_0) and density after sintering (ρ), linear shrinkage (L) and porosity (P)

Sample	H [GPa]	K_{IC} [MPa·m$^{1/2}$]	ρ_0 [g/cm^3]	ρ [g/cm^3]	L [%]	P [vol.%]
H-CS	3.71 ± 0.12	1.19 ± 0.35	1.93	2.79	13.9	7.3
Ag-CS	1.72 ± 0.01	1.25 ± 0.12	1.92	2.25	8.0	25.3
Cu-CS	3.85 ± 0.12	1.46 ± 0.37	1.94	2.78	13.4	8.3
Zn-CS	1.71 ± 0.20	1.01 ± 0.17	1.96	2.34	5.3	23.0
H-MW	3.66 ± 0.25	1.00 ± 0.24	2.03	2.76	13.0	7.6
Ag-MW	3.61 ± 0.06	1.34 ± 0.25	1.89	2.73	11.8	8.8
Cu-MW	3.91 ± 0.09	1.17 ± 0.30	1.83	2.85	12.8	6.9
Zn-MW	1.68 ± 0.26	1.04 ± 0.15	1.85	2.66	10.5	11.3

is known that elongated pores have a more negative influence on the value of H than spherical ones [18]. The impact of P was less pronounced on the values of K_{IC}. Generally, the K_{IC} values are in accordance with the AGS values. The best mechanical properties, the highest values of both H and K_{IC}, were achieved for Cu-doped sample obtained by conventional sintering.

Hitherto, research conducted on ceramics obtained from doped HAp showed also a clear effect of doping on the mechanical properties of the ceramics. Veljović *et al.* [14] used single- and two-step microwave sintering (MWSSS and MWTSS) and conventional single-step sintering (CSSS) to obtain ceramics from Sr- and Mn-doped HAp. The highest values of H showed ceramics sintered by MWSSS at 1200 °C, 4.80 GPa for Sr-HAp and 4.78 GPa for Mn-HAp (K_{IC}: 1.24 and 1.07 MPa·m$^{1/2}$, respectively). The best results for K_{IC} were exhibited by ceramics obtained using MWTSS at 950 °C: 1.54 MPa·m$^{1/2}$ for Sr-HAp and 1.35 MPa·m$^{1/2}$ for Mn-HAp (H: 3.62 and 3.78 GPa, respectively). Curran *et al.* [16] investigated ceramics obtained from Sr-HAp (5 and 10 wt.% of Sr) and sintered by MW and CS for 1 h at 1200 °C. They found that the values of H for the ceramics with 10 wt.% of Sr were about 5 (MW) and 4.5 GPa (CS), and for the ceramics with 5 wt.% of Sr, they were about 4.3 GPa (for both MW and CS), while the pure HAp exhibited 1.7 (MW) and 2.7 GPa (CS). Gunawan *et al.* [25] studied Zn-doped BCP ceramics sintered by CS at 1000 to 1300 °C. The maximum H and K_{IC} values of 3.44 GPa and 1.43 MPa·m$^{1/2}$, respectively, were achieved for the 4 mol% Zn-doped BCP samples sintered at 1200 °C.

In order to obtain a clearer insight into the morphology of ceramics at the beginning of sintering, the fracture surfaces of the samples MW09 were recorded by SEM (Fig. 5). Based on the Fig. 5, it is possible to conclude that in the Ag ceramics there are more hollow spheres of apatite than in the H and Cu ceramics.

Spherical aggregates were formed during hydrothermal synthesis of HAp powders. These spherical aggregates consisted of particles that had stick form, one part of them was full, and the other part hollow. Hollow forms could be seen in Fig. 5 (indicated by the arrows). It could be assumed that some hollow spheres were shattered due to the relatively high pressure during compaction and that some pores remained in the compact between those broken parts. Therefore, this amount of Ag^+ ions during doping lead to the formation of more pores and partially intra- and partially inter-spherical aggregates. In addition, in the sample Ag-MW09 particles were noticeably bigger compared to those in the samples H-MW09 and Cu-MW09, which have a similar structure (Fig. 5).

It is probable that doping of HAp with Zn^{2+} ions affects the formation of a larger number of hollow spheres in the apatite powder, too. In contrast to other compacts, the transformation HAp → TCP in compact made of Zn-HAp powders is faster during the first stage of sintering and obtained structure consisted of weakly connected grains formed out of the spherical aggregates and a large volume of pores remained between them (Fig. 5). When breaking the described ceramics structure, it is easier to separate the grains rather than to cut grains and therefore in the case of Zn-MW09 cavities originating from the hollow spheres cannot be seen.

The porosity formed at the beginning of the sintering, for the samples with Ag and Zn, was later hard to eliminate. These samples exhibited the highest porosity at the end of sintering and consequently the lowest values for H (Table 2).

The samples with Cu, which were formed by compaction of the powder HAp doped with Cu^{2+} ions, showed the best stabilization of β-TCP and minimum P among all the ceramics. Consequently, these samples showed the best results for H and K_{IC} compared to other samples presented in this paper.

The literature indicated that the transformation HAp → α-TCP leads to the formation of blowholes in the structure of apatite [26]. Also, the transformation HAp → TCP generally weakens mechanical properties [28,45]. As already demonstrated, sintering of the ceramics at higher temperatures led to a significant transformation of HAp into TCP. This transformation probably contributes to a weakening of the overall mechanical properties. However, these HAp/β-TCP/α-TCP materials could be very useful as implants in places where the repair of the skeletal system does not need high mechanical properties but rather a rapid propagation of new bone is essential [1]. On the site of the installation of ceramics, the action of the doping ions could be very

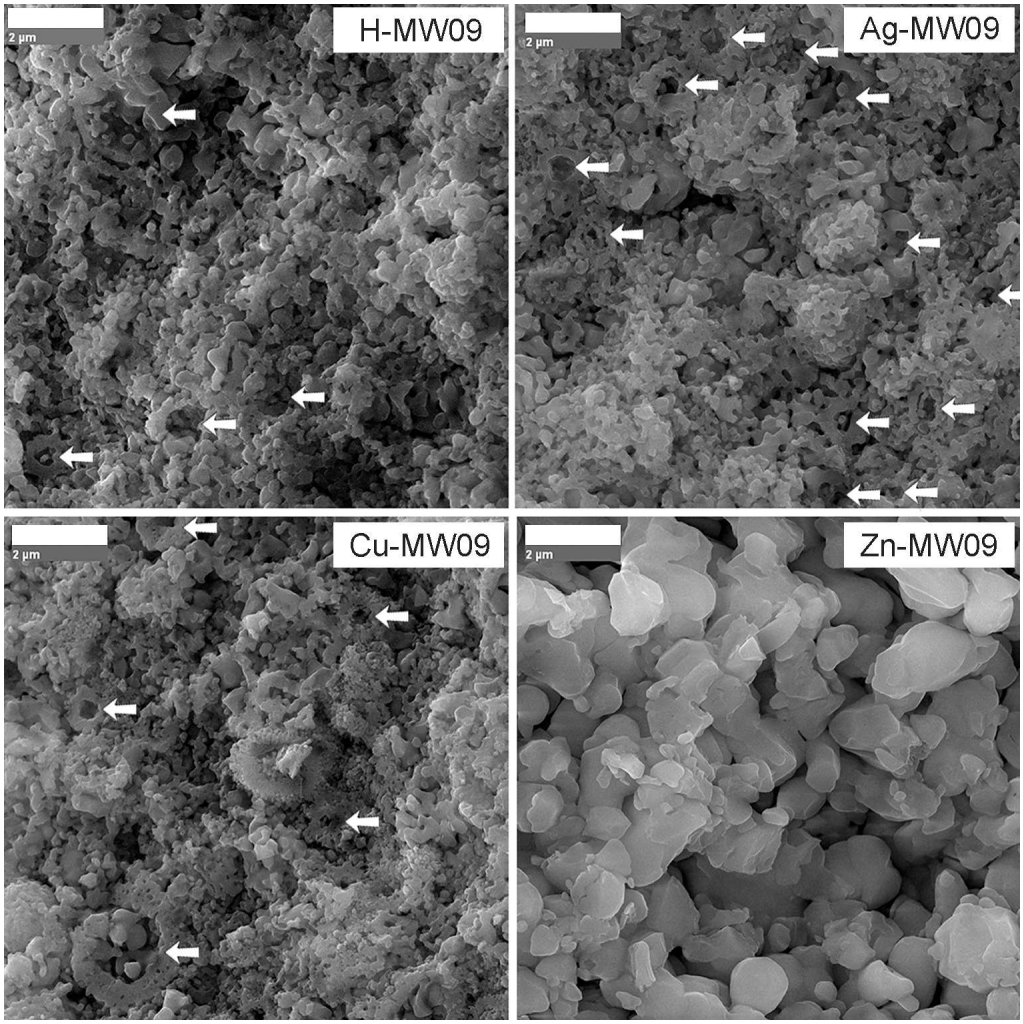

Figure 5. Fractured surfaces of the MW09 samples series (all figures were recorded at 20000× magnification and the marker bar is 2 µm)

important because Ag^+, Cu^{2+} and Zn^{2+} ions are antimicrobial agents and also the latter two ions are micronutrients [34–36,46,47].

IV. Conclusions

Hydrothermally synthesized powders, pure HAp and HAp doped with Ag^+, Cu^{2+} and Zn^{2+} ions, were used to obtain ceramics by conventional (CS) and microwave (MW) sintering at 1200 °C. The sintering led to the spheres merging, but numerous pores between the spheres and intra-pores in the hollow spheres remained in materials. Ag^+ and Zn^{2+} ions have weaken densification of ceramics through the creation of a larger number of pores, which are more difficult to remove during sintering. This significantly impaired the mechanical properties of the ceramics. On the contrary, ceramics with Cu^{2+} ions contained the least pores and consequently, had the best mechanical properties. All the ceramics contained HAp/β-TCP/α-TCP phases in different mass ratios. The ceramics with Cu^{2+} ions consisted mainly of the β-TCP phase. The advantages of MW sintering were confirmed by comparing CS and MW ceramics, through better densification of the samples, although the sample Cu-CS achieved the best combination of values for H and K_{IC} of 3.85 GPa and 1.46 MPa·m$^{1/2}$, respectively.

Acknowledgement: The authors wish to acknowledge the financial support for this research from the Ministry of Education, Science and Technological Development of the Republic of Serbia through projects III 45019 and FP7-REGPOT-2009-1 NANOTECH FTM. The authors would like to thank Dr Aija Krumina (Riga Technical University, Institute of Inorganic Chemistry, Latvia) and Dr. Jelena Pantić (Institute of Nuclear Sciences "Vinča", Serbia) for XRD diffraction experiments.

References

1. S.V. Dorozhkin, "Calcium orthophosphate bioceramics", *Ceram. Int.*, **41** [10] (2015) 13913–13966.
2. E. Champion, "Sintering of calcium phosphate bioceramics", *Acta Biomater.*, **9** [4] (2013) 5855–5875.
3. L.L Hench, "Bioceramics", *J. Am. Ceram. Soc.*, **81** [7] (1998) 1705–1728.
4. S.V. Dorozhkin, "Biphasic, triphasic and multiphasic calcium orthophosphates", *Acta Biomater.*, **8** [3] (2012) 963–977.

5. Y. Xie, D. Chopin, C. Morin, P. Hardouin, Z. Zhu, J. Tang, J. Lu, "Evaluation of the osteogenesis and biodegradation of porous biphasic ceramic in the human spine", *Biomaterials*, **27** [13] (2006) 2761–2767.
6. G. Daculsi, O. Laboux, O. Malard, P. Weiss, "Current state of the art of biphasic calcium phosphate bioceramics", *J. Mater. Sci. Mater. Med.*, **14** [3] (2003) 195–200.
7. M. Descamps, L. Boilet, G. Moreau, A. Tricoteaux, J. Lu, A. Leriche, V. Lardot, F. Cambier, "Processing and properties of biphasic calcium phosphates bioceramics obtained by pressureless sintering and hot isostatic pressing", *J. Eur. Ceram. Soc.*, **33** [7] (2013) 1263–1270.
8. O. Brown, M. McAfee, S. Clarke, F. Buchanan, "Sintering of biphasic calcium phosphates", *J. Mater. Sci. Mater. Med.*, **21** [8] (2010) 2271–2279.
9. A. Chanda, S. Dasgupta, S. Bose, A. Bandyopadhyay, "Microwave sintering of calcium phosphate ceramics", *Mater. Sci. Eng. C*, **29** [4] (2009) 1144–1149.
10. A. Thuault, E. Savary, J.C. Hornez, G. Moreau, M. Descamps, S. Marinel, A. Leriche, "Improvement of the hydroxyapatite mechanical properties by direct microwave sintering in single mode cavity", *J. Eur. Ceram. Soc.*, **34** [7] (2014) 1865–1871.
11. Dj. Veljović, E. Palcevskis, A. Dindune, S. Putić, I. Balać, R. Petrović, Dj. Janaćković, "Microwave sintering improves the mechanical properties of biphasic calcium phosphates from hydroxyapatite microspheres produced from hydrothermal processing", *J. Mater. Sci.*, **45** [12] (2010) 3175–3183.
12. Dj. Veljović, I. Zalite, E. Palcevskis, I. Smiciklas, R. Petrović, Dj. Janaćković, "Microwave sintering of fine grained HAP and HAP/TCP bioceramics", *Ceram. Int.*, **36** [2] (2010) 595–603.
13. S. Dasgupta, S. Tarafder, A. Bandyopadhyay, S. Bose, "Effect of grain size on mechanical, surface and biological properties of microwave sintered hydroxyapatite", *Mater. Sci. Eng. C*, **33** [5] (2013) 2846–2854.
14. Dj. Veljovic, Z. Radovanovic, A. Dindune, E. Palcevskis, A. Krumina, R. Petrović, Dj. Janaćković, "The influence of Sr and Mn incorporated ions on the properties of microwave single- and two-step sintered biphasic HAp/TCP bioceramics", *J. Mater. Sci.*, **49** [19] (2014) 6793–6802.
15. Dj. Veljovic, E. Palcevskis, I. Zalite, R. Petrovic, Dj. Janackovic, "Two-step microwave sintering – A promising technique for the processing of nanostructured bioceramics", *Mater. Lett.*, **93** (2013) 251–253.
16. D.J. Curran, T.J. Fleming, M.R. Towler, S. Hampshire, "Mechanical parameters of strontium doped hydroxyapatite sintered using microwave and conventional methods", *J. Mechan. Behav. Biomed. Mater.*, **4** [8] (2011) 2063–2073.
17. S. Laasri, M. Taha, A. Laghzizil, E.K. Hlil, J. Chevalier, "The affect of densification and dehydroxylation on the mechanical properties of stoichiometric hydroxyapatite bioceramics", *Mater. Res. Bull.*, **45** [10] (2010) 1433–1437.
18. Dj. Veljović, R. Jančić-Hajneman, I. Balać, B. Jokić, S. Putić, R. Petrović, Dj. Janaćković, "The effect of the shape and size of the pores on the mechanical properties of porous HAP-based bioceramics", *Ceram. Int.*, **37** [2] (2011) 471–479.
19. C.Y. Tang, P.S. Uskokovic, C.P. Tsui, Dj. Veljovic, R. Petrovic, Dj. Janackovic, "Influence of microstructure and phase composition on the nanoindentation characterization of bioceramic materials based on hydroxyapatite", *Ceram. Int.*, **35** [6] (2009) 2171–2178.
20. G.E.J. Poinern, R.K. Brundavanam, X.T. Le, D. Fawcett, "The mechanical properties of a porous ceramic derived from a 30 nm sized particle based powder of hydroxyapatite for potential hard tissue engineering applications", *Am. J. Biomed. Eng.*, **2** [6] (2012) 278–286.
21. L.T. Bang, S. Ramesh, J. Purbolaksono, Y.C. Ching, B.D. Long, H. Chandran, S. Ramesh, R. Othman, "Effects of silicate and carbonate substitution on the properties of hydroxyapatite prepared by aqueous co-precipitation method", *Mater. Des.*, **87** (2015) 788–796.
22. M. Lukić, Z. Stojanović, S.D. Škapin, M. Maček-Kržmanc, M. Mitrić, S. Marković, D. Uskoković, "Dense fine-grained biphasic calcium phosphate (BCP) bioceramics designed by two-step sintering", *J. Eur. Ceram. Soc.*, **31** [1–2] (2011) 19–27.
23. J. Wang, L.L. Shaw, "Nanocrystalline hydroxyapatite with simultaneous enhancements in hardness and toughness", *Biomaterials*, **30** [34] (2009) 6565–6572.
24. J. Song, Y. Liu, Y. Zhang, L. Jiao, "Mechanical properties of hydroxyapatite ceramics sintered from powders with different morphologies", *Mater. Sci. Eng. A*, **528** [16-17] (2011) 5421–5427.
25. Gunawan, I. Sopyan, M. Mel, Suryanto, "Investigations of the effects of initial Zn concentration and sintering conditions on the phase behavior and mechanical properties of Zn-doped BCP", *Adv. Environ. Biol.*, **8** [3] (2014) 680–685.
26. M.A. Ahmed, S.F. Mansour, S.I. El-dek, S.M. Abd-Elwahab, M.K. Ahmed, "Characterization and annealing performance of calcium phosphate nanoparticles synthesized by co-precipitation method", *Ceram. Int.*, **40** [8] (2014) 12807–12820.
27. K.T. Chu, S.F. Ou, S.Y. Chen, S.Y. Chiou, H.H. Chou, K.L. Ou, "Research of phase transformation induced biodegradable properties on hydroxyapatite and tricalcium phosphate based bioceramic", *Ceram. Int.*, **39** [2] (2013) 1455–1462.
28. S.F. Ou, S.Y. Chiou, K.L. Ou, "Phase transformation on hydroxyapatite decomposition", *Ceram. Int.*, **39** [4] (2013) 3809–3816.
29. Dj. Veljović, B. Jokić, R. Petrović, E. Palcevskis, A. Dindune, I.N. Mihailescu, Dj. Janaćković, "Processing of dense nanostructured HAP ceramics by sintering and hot pressing", *Ceram. Int.*, **35** [4] (2009) 1407–1413.
30. L. Boilet, M. Descamps, E. Rguiti, A. Tricoteaux, J. Lu, F. Petit, V. Lardot, F. Cambier, A. Leriche, "Processing and properties of transparent hydroxyapatite and β tricalcium phosphate obtained by HIP process", *Ceram. Int.*, **39** [1] (2013) 283–288.
31. S. Li, H. Izui, M. Okano, "Densification, microstructure, and behavior of hydroxyapatite ceramics sintered by using spark plasma sintering", *J. Eng. Mater. Technol.*, **130** [3] (2008) 031012-1–031012-7.
32. S. Lala, T.N. Maity, M. Singha, K. Biswas, S.K. Pradhan, "Effect of doping (Mg, Mn, Zn) on the microstructure and mechanical properties of spark plasma sintered hydroxyapatites synthesized by mechanical alloying", *Ceram. Int.*, **43** [2] (2017) 2389–2397.
33. P. van Landuyt, F. Li, J.P. Keustermans, J.M. Streydio, F. Delannay, E. Muting, "The influence of high sintering tem-

peratures on the mechanical properties of hydroxyapatite", *J. Mater. Sci. Mater. Med.*, 6 [1] (1995) 8–13.
34. Ž. Radovanović, Dj. Veljović, B. Jokić, S. Dimitrijević, G. Bogdanović, V. Kojić, R. Petrović, Dj. Janaćković, "Biocompatibility and antimicrobial activity of zinc(II)-doped hydroxyapatite, synthesized by a hydrothermal method", *J. Serb. Chem. Soc.*, **77** [12] (2012) 1787–1798.
35. Ž. Radovanović, B. Jokić, Dj. Veljović, S. Dimitrijević, V. Kojić, R. Petrović, Dj. Janaćković, "Antimicrobial activity and biocompatibility of Ag^{+}- and Cu^{2+}-doped biphasic hydroxyapatite/α-tricalcium phosphate obtained from hydrothermally synthesized Ag^{+}- and Cu^{2+}-doped hydroxyapatite", *Appl. Surf. Sci.*, **307** (2014) 513–519.
36. M. Šupová, "Substituted hydroxyapatites for biomedical applications: A review", *Ceram. Int.*, **41** [8] (2015) 9203–9231.
37. A.G. Evans, E.A. Charles, "Fracture toughness determination by indentation", *J. Am. Ceram. Soc.*, **59** [7-8] (1976) 371–372.
38. S. Koutsopoulos, "Synthesis and characterization of hydroxyapatite crystals: A review study on the analytical methods", *J. Biomed. Mater. Res.*, **62** [4] (2002) 600–612.
39. S. Pramanik, A.K. Agarwal, K.N. Rai, A. Garg, "Development of high strength hydroxyapatite by solid-state-sintering process", *Ceram. Int.*, **33** [3] (2007) 419–426.
40. I.R. Gibson, I. Rehman, S.M. Best, W. Bonfield, "Characterization of the transformation from calcium-deficient apatite to β-tricalcium phosphate", *J. Mater. Sci. Mater. Med.*, **11** [9] (2000) 533–539.
41. B. Jokić, M. Mitrić, V. Radmilović, S. Drmanić, R. Petrović, Dj. Janaćković, "Synthesis and characterization of monetite and hydroxyapatite whiskers obtained by a hydrothermal method", *Ceram. Int.*, **37** [1] (2011) 167–173.
42. Z. Zyman, D. Rokhmistrov, I. Ivanov, M. Epple, "The influence of foreign ions on the crystal lattice of hydroxyapatite upon heating", *Mater. Wiss. Werkst.*, **37** [6] (2006) 530–532.
43. A. Banerjee, A. Bandyopadhyay, S. Bose, "Hydroxyapatite nanopowders: synthesis, densification and cell-materials interaction", *Mater. Sci. Eng. C*, **27** [4] (2007) 729–735.
44. E.R. Nightingale Jr., "Phenomenological theory of ion salvation. Effective radii of hydrated ions", *J. Phys. Chem.*, **63** [9] (1959) 1381–1387.
45. Y.W. Gua, K.A. Khora, P. Cheang, "Bone-like apatite layer formation on hydroxyapatite prepared by spark plasma sintering (SPS)", *Biomaterials*, **25** [18] (2004) 4127–4134.
46. V. Stanić, S. Dimitrijević, J. Antić-Stanković, M. Mitrić, B. Jokić, I.B. Plećaš, S. Raičević, "Synthesis, characterization and antimicrobial activity of copper and zinc-doped hydroxyapatite nanopowders", *Appl. Surf. Sci.*, **256** [20] (2010) 6083–6089.
47. V. Stanić, Dj. Janaćković, S. Dimitrijević, S.B. Tanasković, M. Mitrić, M.S. Pavlović, A. Krstić, D. Jovanović, S. Raičević, "Synthesis of antimicrobial monophase silver-doped hydroxyapatite nanopowders for bone tissue engineering", *Appl. Surf. Sci.*, **257** [9] (2011) 4510–4518.